7-2017

Time Optimal State Feedback Control with Application to a Spacecraft with Cold Gas Propulsion

Samuel J. Kitchen-McKinley
Embry-Riddle Aeronautical University, kitchens@my.erau.edu

Sergey V. Drakunov
Embry Riddle Aeronautical University, drakunov@erau.edu

Available online at www.sciencedirect.com

ScienceDirect

IFAC Papers Online CONFERENCE PAPER ARCHIVE

IFAC PapersOnLine 50-1 (2017) 7223–7228

Time Optimal State Feedback Control with Application to a Spacecraft with Cold Gas Propulsion ⋆

Samuel J. Kitchen-McKinley * **Sergey V. Drakunov** *

* *Physical Science Department, Embry-Riddle Aeronautical University, Daytona Beach, FL 32114 USA (e-mail: kitchens@my.erau.edu, drakunov@erau.edu).*

Abstract: A cold gas propulsion system is well suited to provide the required thrust for a small surveyor spacecraft operated near an asteroid or planetary surface. The cold gas propellant can obtained in-situ from local surface or atmospheric constituents. For small spacecraft, the cold gas system may be limited to only on-off control of the main tank where the generated thrust is directly dependent on the tank pressure. As such the thrust will slowly decrease as the propellant is expended. A state feedback, time optimal, control law is developed for a vehicle with decreasing thrust in translational motion. The success of the control law is shown in simulation.

Keywords: Control of systems in vehicles, Guidance, navigation and control of vehicles, Space exploration and transportation, Optimal control theory, Variable structure control

1. INTRODUCTION

Cold gas propulsion is a relatively low cost, low mass, and simple propulsion system that can be run with many kinds of benign propellants at low power consumption levels. Such a method of propulsion is a space proven technology that has been in use since the 1960's. Because of the relatively low thrust levels and high response times, cold gas propulsion systems have been mainly used for station keeping and attitude control systems. See Mueller et al. (2010).

As spacecraft become smaller, cheaper and more numerous, cold gas propulsion is a simple option for main propulsion. CubeSats, for example, are a popular low cost spacecraft used for LEO missions. For CubeSats, cold gas propulsion offers low mass, low energy and benign propellants, giving the spacecraft accurate orbital and attitude control. Cold gas microthrusters have been in development for such small sized spacecraft as seen in Kvell et al. (2014).

For missions beyond LEO, small free flying vehicles may be used for surveying planetary surfaces. In order to extent the life of future planetary exploration missions, it becomes necessary to use In-Situ Resource Utilization (ISRU). ISRU technology is currently in development for human and robotic missions to the Moon, Mars, and near Earth asteroids, to be able to extract resources such as water, oxygen, propellants, and building materials from the local target environment. This not only saves cost from launch mass, but makes exploration missions more flexible and can prolong a mission's life indefinitely. See Sanders and Larson (2013).

⋆ This work was supported by NASA SBIR/STTR Phase II grant for the Free-Flying Unmanned Robotic Spacecraft for Asteroid Resource Prospecting and Characterization project under contract NNX15CK07C.

For a small spacecraft operating in a low gravity environment, a cold gas propulsion system can be used as the main propulsion system for translation and attitude control despite its relatively low thrust. Using only the gas pressure as the stored potential energy, cold gas propulsion expands the number of types of materials that can be locally collected as propellant. Because the cold gas propellant can be collected locally, the low specific impulse of cold gas propulsion does not have to be a limiting factor for the lifetime of a mission.

The primary components of a cold gas propulsion system include a high pressure propellant storage vessel, a regulator to down step and provide a constant downstream pressure, solenoid valves for fast on/off switching, and thrusters to accelerate gas flow. See Makled et al. (2009), Anis (2012), and Furumo (2013). A general, single stream schematic of a cold gas propulsion system is shown in Figure 1.

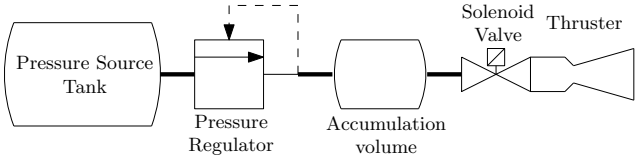

Fig. 1. General cold gas propulsion system

For this constant thrust system, previous control methods have focused on thrust control using gas flow control, such as in Kvell et al. (2014), or pulse modulation of the solenoid valve, such as in Kienitz and Bals (2005). The constant thrust also allows classical optimal control analysis, Kirk (2004), for spacecraft motion.

However, the simplest configuration for a cold gas system may be a control valve and thruster nozzle attached directly to a pressure tank. This further reduces the

Peer review under responsibility of International Federation of Automatic Control.
10.1016/j.ifacol.2017.08.1366

complexity of the propulsion system, but also reduces the controllability. The cold gas propulsion system fluid model is presented as the motivation and derivation of a system where the thrust force is directly dependent on the remaining fuel. A feedback control method is developed in general for such a class of systems with this fuel dependency. The control law derivation derivation is shown on a simplified example of this class of systems so show the steps more clearly. The control law is time optimal accounting for fuel constraints and control input actuator constraints.

2. COLD GAS MODEL

To understand the relationship between the cold gas propulsion system and the thrust it generates, the cold gas model is presented from Kitchen-McKinley et al. (2016). The cold gas system is modeled as one dimensional, isentropic, fluid flow, using a series of control volumes connected by orifices.

2.1 Control volume

In each control volume, the pressure is governed by the ideal gas law. The connecting orifices will determine the mass flow between each control volume. The ideal gas law is given as,

$$PV = mRT \tag{1}$$

where P is pressure, V is volume, m is mass, and T is temperature, of the gas, and R is the specific gas constant. The volumes are constant and the temperatures are considered constant as the pressure changes in the tank are slow relative to heat exchange with the environment. This can be seen experimentally in Hashem (2004). Taking the time derivative of (1) yields

$$\dot{P} = \frac{RT}{V}\dot{m} \tag{2}$$

The total mass flow rate, $\frac{dm}{dt} = \dot{m}$, is the sum of mass flow in and out of each volume as

$$\dot{m} = \sum \dot{m}_{in} - \sum \dot{m}_{out} \tag{3}$$

2.2 Orifice flow

For isentropic, quasi-steady-state, subsonic flow through an orifice, the mass flow rate is given by

$$\dot{m} = \frac{AP_u}{(\gamma-1)^{\frac{1}{2}}}\sqrt{\frac{2\gamma}{RT_u}\left[\left(\frac{P_d}{P_u}\right)^{\frac{2}{\gamma}} - \left(\frac{P_d}{P_u}\right)^{\frac{\gamma+1}{\gamma}}\right]} \tag{4}$$

where subscripts u and d represent the upstream and downstream conditions respectively, A is the cross sectional area of the orifice, and $\gamma = \frac{c_p}{c_v}$ is the ratio of specific heats of the gas.

Regulator A regulator consists of a series of orifice flow points and control volumes. In order to maintain a constant downstream pressure, the regulator employs a variable downstream control volume that depends directly on the difference between a reference pressure and downstream pressure. The dynamics of the regulator can be described as a variable orifice area that controls the downstream pressure as

$$\tau_r \dot{A}_r = -A_r - k_r(P_d - P_r) \tag{5}$$

with two constant parameters, τ_r, and k_r, where A_r is the orifice area, P_d is the downstream pressure and P_r is the manually controlled reference pressure.

Solenoid valve The solenoid valve provides the control input to the cold gas system. The solenoid valve area is determined by an electrically driven poppet. The poppet is either fully closed or fully open depending on an the applied voltage. The valve area is therefore either zero or maximum, and maximum area will allow the chamber pressure of the thruster to be based on the upstream pressure. The control input is therefore limited to be commanded as either open or closed.

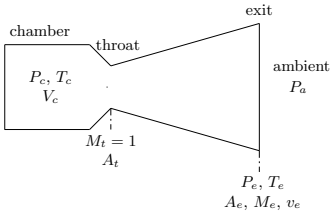

Fig. 2. Converging diverging nozzle

Nozzle A converging-diverging nozzle can accelerate the gas through isentropic expansion. Under the supersonic condition given when, $\frac{P_c}{P_a} \geq \left(\frac{\gamma+1}{2}\right)^{\frac{\gamma}{\gamma-1}}$, the pressure differential is large enough such that the gas flow will be choked at the throat and accelerated to be supersonic at the exit. The exit conditions can be calculated from the following rocket thrust equations,

$$\frac{A_e}{A_t} = \frac{1}{M_e}\sqrt{\left(\frac{2}{\gamma+1}\right)\left(1+\frac{\gamma-1}{2}M_e^2\right)^{\frac{\gamma+1}{\gamma-1}}} \tag{6}$$

$$\frac{P_e}{P_c} = \left(1+\frac{\gamma-1}{2}M_e^2\right)^{-\frac{\gamma}{\gamma-1}} \tag{7}$$

$$\frac{T_e}{T_c} = \left(1+\frac{\gamma-1}{2}M_e^2\right)^{-1} \tag{8}$$

$$v_e = M_e\sqrt{\gamma R T_e} \tag{9}$$

where $\epsilon = \frac{A_e}{A_t}$ is the cross section area expansion ratio, v is the gas velocity, M is the mach number, subscript c, t , and e represent the chamber, throat, and exit conditions, respectively, and P_a is the ambient pressure. These variables are also labeled in Figure 2. The mass flow rate and the thrust force, F, are then calculated as

$$\dot{m} = A_t P_c\sqrt{\frac{\gamma}{RT_c}\left(\frac{2}{\gamma+1}\right)^{\frac{\gamma+1}{\gamma-1}}} \tag{10}$$

$$F = \dot{m}v_e + (P_e - P_a)A_e \tag{11}$$

See Sutton and Biblarz (2001).

3. FULL SYSTEM MODEL

For a spacecraft in a low gravity environment the cold gas propulsion system will have two main thrusters to provide

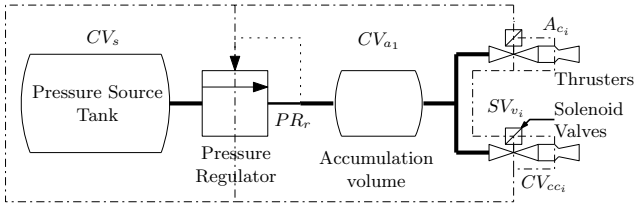

Fig. 3. Constant thrust cold gas propulsion schematic. The dot dash lines show control volumes. Each control volume and orifice is labeled and the nomenclature is given in Table 1.

thrust in each direction for translational motion in each dimension. Two configurations are presented. A propulsion system which provides constant thrust, and a less complex propulsion system which directly feeds the tank pressure to produce thrust.

3.1 Constant thrust

For one-dimensional motion the schematic for a constant thrust system is shown in Figure 3. The pressure regulator allows a preset constant downstream pressure, and the solenoid valve allows for two states, zero or max thrust.

Table 1. component subscript labels

Control Volumes	
CV_s	source
CV_{a_1}	accumulation volume 1
CV_{cc_i}	thruster chamber $i = 1, 2$
Orifices	
PR_r	pressure regulator 1
SV_{v_i}	solenoid valve $i = 1, 2$
A_{c_i}	thruster throat area $i = 1, 2$

Using (2),(3),(4),(5) and (10) for each component labeled in Figure 3, the model becomes a system of first order differential equations given as the following,

$$\dot{P}_s = \frac{RT_s}{V_s}(-\dot{m}_r) \tag{12a}$$

$$\dot{m}_r = \frac{A_r P_s}{(\gamma-1)^{\frac{1}{2}}}\sqrt{\frac{2\gamma}{RT_s}\left[\left(\frac{P_{a_1}}{P_s}\right)^{\frac{2}{\gamma}} - \left(\frac{P_{a_1}}{P_s}\right)^{\frac{\gamma+1}{\gamma}}\right]} \tag{12b}$$

$$\tau_r \dot{A}_r = -A_r - k_r(P_{a_1} - P_r) \tag{12c}$$

$$\dot{P}_{a_1} = \frac{RT_{a_1}}{V_{a_1}}(\dot{m}_r - \sum_{i=1}^{2}\dot{m}_{v_i}) \tag{12d}$$

$$\dot{m}_{v_i} = \frac{u_i A_{v_i} P_{a_1}}{(\gamma-1)^{\frac{1}{2}}}\sqrt{\frac{2\gamma}{RT_{a_1}}\left[\left(\frac{P_{cc_i}}{P_{a_1}}\right)^{\frac{2}{\gamma}} - \left(\frac{P_{cc_i}}{P_{a_1}}\right)^{\frac{\gamma+1}{\gamma}}\right]} \tag{12e}$$

$$\dot{P}_{cc_i} = \frac{RT_{cc_i}}{V_{cc_i}}(\dot{m}_{v_i} - \dot{m}_{c_i}) \tag{12f}$$

$$\dot{m}_{c_i} = A_{c_i} P_{cc_i}\sqrt{\frac{\gamma}{RT_{cc_i}}\left(\frac{2}{\gamma+1}\right)^{\frac{\gamma+1}{\gamma-1}}} \tag{12g}$$

where u_i is the solenoid control input for the thrusters. The control input is restricted so that only one can fire at a time, given that both valves open will cancel the generated thrust.

3.2 Direct Feed

For one-dimensional motion the schematic for a direct feed system is shown in Figure 4. This is the least complex version of a cold gas system. With the nozzle attached directly to a pressure tank, the tank pressure becomes the thruster chamber pressure, and so the thrust is directly dependent on the tank pressure state which decreases when used.

This system reduces the component complexity but it increases the order of state equations needed to determine optimal control. Again, using (2),(3),(4),(5) and (10) for

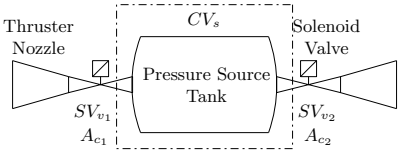

Fig. 4. Direct feed cold gas propulsion schematic. The dot dash lines show control volumes. Each control volume and orifice is labeled and the nomenclature is given in Table 1.

each component labeled in Figure 3, the model becomes a system of first order differential equations given as,

$$\dot{P}_s = \frac{RT_s}{V_s}(-\sum_{i=1}^{2}\dot{m}_{c_i}) \tag{13a}$$

$$\dot{m}_{c_i} = u_i A_{c_i} P_s\sqrt{\frac{\gamma}{RT_s}\left(\frac{2}{\gamma+1}\right)^{\frac{\gamma+1}{\gamma-1}}} \tag{13b}$$

where u_i is the solenoid control input for each thruster, as $i = 1, 2$ represents each thruster. Again, the control input is restricted so that only one can fire at a time.

3.3 Spacecraft model

The one dimensional motion of the spacecraft will be governed by the following system

$$\begin{aligned}\dot{x}_1 &= x_2\\ \dot{x}_2 &= F\end{aligned} \tag{14}$$

where x_1 is position, x_2 is velocity, and F is the thrust force. The thrust force can be written in terms of the fuel pressure by substituting (6)-(10) into (11), as

$$F = u_i A_c\left(\left[\gamma M_e\left(\frac{2}{\gamma+1}\right)^{\frac{\gamma+1}{2(\gamma-1)}}\left(1+\frac{\gamma-1}{2}M_e^2\right)^{-\frac{1}{2}} + \epsilon\left(1+\frac{\gamma-1}{2}M_e^2\right)^{-\frac{\gamma}{\gamma-1}}\right]P_s - \epsilon P_a\right) \tag{15}$$

To obtain the closed loop pressure dynamics, substitute (13b) into (13a) to get

$$\dot{P}_s = -|u| A_c P_s\sqrt{\frac{\gamma RT_s}{V_s^2}\left(\frac{2}{\gamma+1}\right)^{\frac{\gamma+1}{\gamma-1}}} \tag{16}$$

where the control input, u, is allowed to take one of three states given as

$$u = \begin{cases} +1 \text{ for } u_1 = 1 \\ 0 \text{ for } u_1, u_2 = 0 \\ -1 \text{ for } u_2 = 1 \end{cases} \tag{17}$$

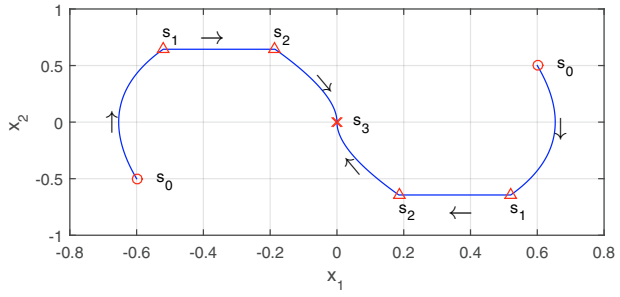

Fig. 5. State space trajectories projected into the x_1 x_2 plane. The points s_0, s_1, s_2, and s_3, represent the control state switching points.

Introducing the thrust dynamics from (15) and (16), (14) can be rewritten, with P_s being denoted as x_3 in state space, as

$$\begin{aligned} \dot{x}_1 &= x_2 \\ \dot{x}_2 &= u f_1(x_3) \\ \dot{x}_3 &= -|u| f_2(x_3) \end{aligned} \tag{18}$$

where

$$\begin{aligned} f_1(x_3) =& A_c \left(\left[\gamma M_e \left(\frac{2}{\gamma+1} \right)^{\frac{\gamma+1}{2(\gamma-1)}} \left(1 + \frac{\gamma-1}{2} M_e^2 \right)^{-\frac{1}{2}} \right. \right. \\ & \left. \left. + \epsilon \left(1 + \frac{\gamma-1}{2} M_e^2 \right)^{-\frac{\gamma}{\gamma-1}} \right] x_3 - \epsilon P_a \right) \end{aligned} \tag{19}$$

$$f_2(x_3) = A_c x_3 \sqrt{\frac{\gamma R T_s}{V_s^2} \left(\frac{2}{\gamma+1} \right)^{\frac{\gamma+1}{\gamma-1}}} \tag{20}$$

The following section will develop a control method for such a class of systems as presented in (18).

4. CONTROL

To develop the method for determining the time optimal control law, the simplest form of (18) is used as an example when $f_1(x_3) = f_2(x_3) = x_3$. The nonlinear, non affine model is then written as

$$\begin{aligned} \dot{x}_1 &= x_2 \\ \dot{x}_2 &= u x_3 \\ \dot{x}_3 &= -|u| x_3 \end{aligned} \tag{21}$$

The control input has three discrete possible states

$$u = \begin{cases} +1 \text{ for } k = 1 \\ 0 \text{ for } k = 2 \\ -1 \text{ for } k = 3 \end{cases} \tag{22}$$

Making the model bilinear in the form $\dot{\mathbf{x}} = A\mathbf{x}$, for $\mathbf{x} = [x_1\ x_2\ x_3]^T$, where

$$A_{u_k} = \begin{bmatrix} 0 & 1 & 0 \\ 0 & 0 & -u_k \\ 0 & 0 & -|u_k| \end{bmatrix} \tag{23}$$

The solution for this differential equation is $\mathbf{x}_f = e^{At_f}\mathbf{x}_i$. There are three possible trajectories, one for each controller state. Let Δt_+ be the time accelerating towards $x_1 = 0$, the path from s_0 to s_1 as shown in Figure 5. Let Δt_0 be the time coasting towards $x_1 = 0$, the path from s_1 to s_2 as shown in Figure 5. Let Δt_- be the time decelerating towards $x_1 = 0$, the path from s_2 to s_3 as shown in Figure 5. For region $x_1 > 0$, these trajectories can be solved as

$$\mathbf{x}_1 = e^{A_{u_-}\Delta t_+}\mathbf{x}_0 \tag{24}$$

$$\mathbf{x}_2 = e^{A_{u_0}\Delta t_0}\mathbf{x}_1 \tag{25}$$

$$\mathbf{x}_3 = e^{A_{u_+}\Delta t_-}\mathbf{x}_2 \tag{26}$$

where $\mathbf{x}_0 = [x_{1_0}\ x_{2_0}\ x_{3_0}]^T$ is the initial system state at point s_0, $\mathbf{x}_1 = [x_{1_1}\ x_{2_1}\ x_{3_1}]^T$ is the system state at switching point s_1, $\mathbf{x}_2 = [x_{1_2}\ x_{2_2}\ x_{3_2}]^T$ is the system state at switching point s_2, and $\mathbf{x}_3 = [x_{1_3}\ x_{2_3}\ x_{3_3}]^T$ is the final system state at point s_3.

The goal is to drive the spacecraft from any initial position $x_1 = x_{10}$, to the desired position $x_1 = 0$. Therefore, to derive the optimal path, we begin at the origin, by finding the region such that applying deceleration at any point in the region will result in a trajectory that will cross the origin $(x_1, x_2 = 0)$. This is begun by solving and evaluating (24) as, $\mathbf{x}_2 = [e^{A_{u_+}\Delta t_-}]^{-1}\mathbf{x}_3$, where the final desired state is $\mathbf{x}_3 = [0\ ,\ 0\ ,\ x_{3_3} \geq 0]^T$. The result is the system ending at point s_3 and beginning at s_2 as

$$\begin{aligned} x_{1_2} &= x_{3_3}\left(e^{\Delta t_-} - 1 - \Delta t_-\right) \\ x_{2_2} &= x_{3_3}\left(1 - e^{\Delta t_-}\right) \\ x_{3_2} &= x_{3_3}\left(e^{\Delta t_-}\right) \end{aligned} \tag{27}$$

System (27) is a set of parametric equations that can be manipulated to remove the parameters, x_{3_3} and Δt_-, and be written into one equation as

$$\sigma_2(\mathbf{x}) = x_1 + x_2 + (x_3 + x_2)\ln\left(\frac{x_3}{x_3 + x_2}\right) \tag{28}$$

where $\sigma_2(\mathbf{x}) = 0$ is a surface in state space such that decelerating from any point on that surface will pass through the desired final state. System (27) can also be used to determine the time spent decelerating on that surface as

$$\Delta t_-(x_{2_2}, x_{3_2}) = \ln\left(\frac{x_{3_2}}{x_{3_2} + x_{2_2}}\right) \tag{29}$$

Next we look at the system coasting towards the surface $\sigma_2(\mathbf{x}) = 0$ from any point in the positive x_1 direction denoted by moving from point s_1 to s_2. Evaluating (25) results in the following parametric equations,

$$\begin{aligned} x_{1_2} &= x_{1_1} + x_{2_1}\Delta t_0 \\ x_{2_2} &= x_{2_1} \\ x_{3_2} &= x_{3_1} \end{aligned} \tag{30}$$

The coasting time from point $\mathbf{x}_1$ to the surface $\sigma_2(\mathbf{x}_2) = 0$ can be found by substituting (30) into (28) and solving for Δt_0. Similarly, the deceleration time can be reevaluated as a function of $\mathbf{x}_1$ by substituting (30) into (29) giving the following equations

$$\begin{aligned} \Delta t_0(\mathbf{x}_1) = -\frac{1}{x_{2_1}} \Bigg[& x_{1_1} + x_{2_1} \\ & + (x_{3_1} + x_{2_1})\ln\left(\frac{x_{3_1}}{x_{3_1} + x_{2_1}}\right) \Bigg] \end{aligned} \tag{31}$$

$$\Delta t_-(\mathbf{x}_1) = \ln\left(\frac{x_{3_1}}{x_{3_1} + x_{2_1}}\right) \tag{32}$$

Lastly, we want to define the coasting and deceleration times as functions of the initial state, $\mathbf{x}_0$, and the time, Δt_+, spent accelerating from point s_0 to s_1. The accelerating system can be found by evaluating (26) resulting in,

$$\begin{aligned} x_{1_1} &= x_{1_0} + x_{2_0}\Delta t_+ - x_{3_0}\left(e^{-\Delta t_+} + \Delta t_+ - 1\right) \\ x_{2_1} &= x_{2_0} + x_{3_0}\left(e^{-\Delta t_+} - 1\right) \\ x_{3_1} &= x_{3_0}\left(e^{-\Delta t_+}\right) \end{aligned} \tag{33}$$

We can now substitute (33) into (31) and (32) to get,

$$\begin{aligned} &\Delta t_0(\mathbf{x}_0, \Delta t_+) = \\ &-\frac{1}{x_{2_0} + x_{3_0}(e^{-\Delta t_+} - 1)}\left[x_{1_0} + x_{2_0} + (x_{3_0} - x_{2_0})\Delta t_+ \right. \\ &\left. + \left(x_{2_0} + x_{3_0}(2e^{-\Delta t_+} - 1)\right)\ln\left(\frac{x_{3_0}e^{-\Delta t_+}}{x_{2_0} + x_{3_0}(2e^{-\Delta t_+} - 1)}\right)\right] \end{aligned} \tag{34}$$

$$\Delta t_-(\mathbf{x}_0, \Delta t_+) = \ln\left(\frac{x_{3_0}e^{-\Delta t_+}}{x_{2_0} + x_{3_0}(2e^{-\Delta t_+} - 1)}\right) \tag{35}$$

The total time, Δt, from point s_0 to s_3 is the sum of times during each leg, written as

$$\Delta t(\mathbf{x}_0, \Delta t_+) = \Delta t_-(\mathbf{x}_0, \Delta t_0) + \Delta t_0(\mathbf{x}_0, \Delta t_0) + \Delta t_+ \tag{36}$$

Note that from the analysis resulting in (34) and (35), it is shown that total time is dependent only on the initial position $\mathbf{x}_0$, and the time spent accelerating away from the initial point, Δt_+. We now have a goal to minimize the total time using our one free parameter Δt_+.

To determine the time optimal surface for switching from accelerating to coasting, we can analyze how the total time changes with a change in acceleration time and evaluate at the boundary as

$$\left.\frac{d\Delta t}{d\Delta t_+}\right|_{\Delta t_+ = 0} = 0 \tag{37}$$

This results in the switching surface

$$\begin{aligned} \sigma_0(\mathbf{x}) = \frac{x_3}{{x_2}^2}\left[x_1 + \frac{x_3 - x_2}{x_3 + x_2}x_2 \right. \\ \left. + (x_3 - x_2)\ln\left(\frac{x_3}{x_3 + x_2}\right)\right] = 0 \end{aligned} \tag{38}$$

Note that for classical time optimal control the solution is bang-bang, where there is constant acceleration and deceleration with no coasting. If this were the case, the analysis would have found $\sigma_0 \equiv \sigma_2$. However, in this case, we have found that it is always time optimal to coast for some time. This has to do with the nature of the system as the acceleration is dependent on the decreasing fuel source.

One more switching surface is required to address the remaining fuel constraint for the case when you want to arrive at the origin with a desired fuel amount, stated as $x_{3_f} \geq x_{3_{\min}}$. This can be accomplished by analyzing the relation of $\frac{dx_2}{dx_3}$ from system (21) for decelerating towards the final state.

$$\int_{x_{2_0}=x_2}^{x_{2_f}=0} dx_2 = -\int_{x_{3_0}=3_2}^{x_{3_f}=x_{3_{\min}}} dx_3 \tag{39}$$

The final surface is

$$\sigma_1(\mathbf{x}) = x_3 - x_{3_{\min}} + x_2 = 0 \tag{40}$$

To complete and combine the analysis for the region $x_1 < 0$, apply the transformation $(\cdot) \rightarrow -\text{sign}(x_2)(\cdot)$ to $\{x_1, x_2, \sigma_0, \sigma_2\}$. Note that, $\text{sign}(\cdot)\text{sign}(\cdot) = 1$, and, $\text{sign}(x_2)x_2 = |x_2|$. We can now write each switching surface in all regions as

$$\begin{aligned} \sigma_0(\mathbf{x}) = \frac{x_3}{{x_2}^2}\left[x_1 + \frac{x_3 + |x_2|}{x_3 - |x_2|}x_2 \right. \\ \left. -\text{sign}(x_2)(x_3 + |x_2|)\ln\left(\frac{x_3}{x_3 - |x_2|}\right)\right] = 0 \end{aligned} \tag{41}$$

$$\sigma_1(\mathbf{x}) = x_3 - x_{3_{\min}} - |x_2| = 0 \tag{42}$$

$$\begin{aligned} \sigma_2(\mathbf{x}) = x_1 + x_2 \\ - \text{sign}(x_2)(x_3 - |x_2|)\ln\left(\frac{x_3}{x_3 - |x_2|}\right) = 0 \end{aligned} \tag{43}$$

These switching surfaces can be visualized in Figure 6.

A control law developed based on these switching surface will be state feedback, time optimal, and fuel constrained.

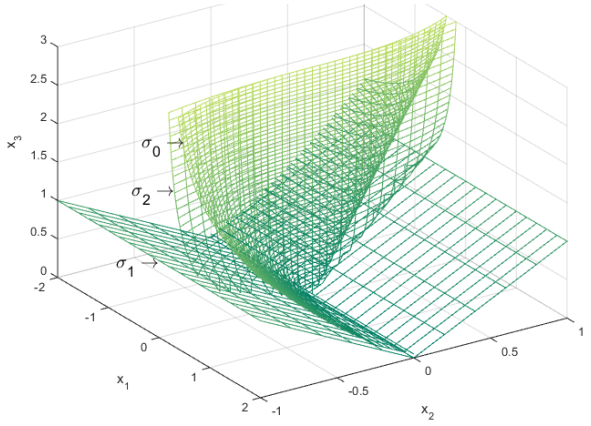

Fig. 6. All three switching surfaces shown in three dimensional state space.

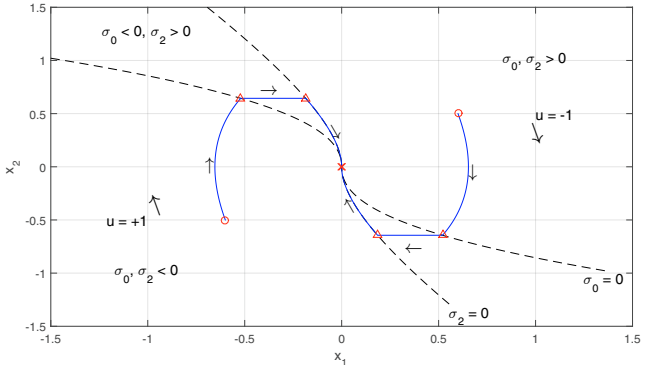

Fig. 7. State space trajectories projected into the x_1 x_2 plane. Trajectories shown for each of the three control states in relation to the switching surfaces. Switching surfaces σ_0 and σ_2 positive and negative regions shown.

The surfaces $\sigma_0(\mathbf{x}) = 0$ and $\sigma_2(\mathbf{x}) = 0$ have their positive and negative regions defined in Figure 7. The surface $\sigma_1(\mathbf{x}) = 0$ is defined as positive in the region above the surface in the positive x_3 direction. From this the control law is designed in a concise form to generate the correct value based only on the states as

$$u = \begin{cases} -\frac{1}{2}[\text{sign}(\sigma_0(\mathbf{x})) + \text{sign}(\sigma_2(\mathbf{x}))] & \text{if } \sigma_1(\mathbf{x}) > 0 \\ -\frac{1}{2}[\text{sign}(x_2) + \text{sign}(\sigma_2(\mathbf{x}))] & \text{if } \sigma_1(\mathbf{x}) \leq 0 \end{cases} \tag{44}$$

From the analysis resulting in (42), in order to reach the origin, the desired remaining fuel, $x_{3_{\min}}$, must be chosen within the range

$$0 \leq x_{3_{\min}} < x_{3_0} - |x_{2_0}| \tag{45}$$

And the origin is not accessible from the region where

$$x_{3_0} - |x_{2_0}| < 0 \tag{46}$$

5. SIMULATION

The model given in (21) using the control law given in (44) is simulated in Matlab and Simulink with initial conditions $\mathbf{x}_0 = [0.6\ ,\ 0.5\ ,\ 2.5]^T$ and desired conditions $\mathbf{x}_{\text{des}} = [0\ ,\ 0\ ,\ \geq 0]^T$.

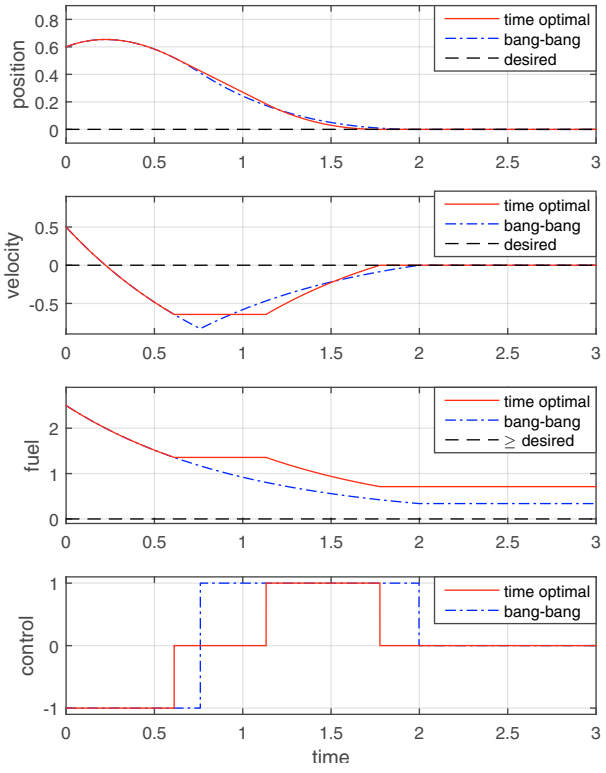

Fig. 8. Time series of systems states and control input shows time optimal, bang-off-bang, control, placing the spacecraft at the desired position with the fuel remaining above its desired value. Bang-bang control is also shown for comparison.

Figure 8 shows the successful convergence of the position to the desired value using each of the three control states only once. There is an acceleration phase towards the origin, a coasting phase, and a deceleration phase to finally come to a stop at the origin. The total maneuver is completed with more fuel remaining than required.

6. CONCLUSION

Cold gas propulsion is a viable system for many spacecraft, including the reduced complexity of the direct feed configuration. This system provided the motivation to analyze such class of systems where the remaining fuel directly impacted the control thrust that could be applied. The results showed that it is possible to develop a time optimal state feedback control law for such a system.

Classical time optimal analysis for a system with constant thrust will result in a bang-bang control profile with one switching point from acceleration to deceleration. Classical fuel optimal analysis for a constant thrust system will result in a bang-off-bang control profile for acceleration, coasting, and then deceleration. However, optimal analysis for the direct feed system found that the switching surface for bang-bang was neither time optimal nor fuel optimal. This can also be seen in Figure 8. It turned out that a coasting period was always time optimal, so a second surface was derived to find the time optimal coasting region. Consequently, by shifting from bang-bang to bang-off-bang, total fuel used was also reduced as well as the total time.

Future work includes generalizing the control development method in terms of any function $f_1(x_3)$ and $f_2(x_3)$ for system 18, including linear and nonlinear functions, and expanding the optimal feedback control for spacecraft attitude and translation control in all three dimensions.

REFERENCES

Anis, A. (2012). Cold Gas Propulsion System An Ideal Choice for Remote Sensing Small Satellites. In B. Escalante (ed.), *Remote Sensing - Advanced Techniques and Platforms*, chapter 20. InTech.

Furumo, J.G. (2013). Cold-gas Propulsion for Small Satellite Attitude Control, Station Keeping, and Deorbit.

Hashem, A. (2004). Design and testing of a cold gas system. In *4th International Spacecraft Propulsion ...*.

Kienitz, K.H. and Bals, J. (2005). Pulse modulation for attitude control with thrusters subject to switching restrictions. *Aerospace Science and Technology*, 9(7), 635–640.

Kirk, D.E. (2004). *Optimal Control Theory: An Introduction*. Dover Publications, Mineola, New York.

Kitchen-McKinley, S.J., Drakunov, S.V., Mueller, R.P., and DuPuis, M.A. (2016). Modeling and Control of Cold Gas Propulsion for Spacecraft Attitude Control. In *ASCE Earth and Space*. ASCE, Orlando, FL.

Kvell, U., Puusepp, M., Kaminski, F., Past, J.E., Palmer, K., Grönland, T.A., and Noorma, M. (2014). Nanosatellite orbit control using MEMS cold gas thrusters. *Proceedings of the Estonian Academy of Sciences*, 63(2S), 279–285.

Makled, A.E., AL-Sanabawy, M.A., and Bakr, M.A. (2009). Theoretical and Experimental Evaluation of Cold Gas System Components. In *Aerospace Sciences & Aviation Technology*, 1–17.

Mueller, J., Hofer, R., and Ziemer, J. (2010). Survey of propulsion technologies applicable to cubesats. In *Joint Army-Navy-NASA-Air Force (JANNAF)*, 1–58. Jet Propulsion Laboratory, National Aeronautics and Space Administration, Colorado Springs, Colorado.

Sanders, G.B. and Larson, W.E. (2013). Progress Made in Lunar In Situ Resource Utilization under NASA ' s Exploration Technology and Development Program.

Sutton, G.P. and Biblarz, O. (2001).